Applied Thermal Engineering 50 (2013) 805–815

Contents lists available at SciVerse ScienceDirect

Applied Thermal Engineering

journal homepage: www.elsevier.com/locate/apthermeng

Experimental evaluation of the performance of a flameless combustor

Amândio Rebola, Mário Costa*, Pedro J. Coelho

Mechanical Engineering Department, Instituto Superior Técnico, Technical University of Lisbon, Avenida Rovisco Pais, 1049-001 Lisbon, Portugal

HIGHLIGHTS

- In the present combustor is possible to establish flameless conditions over a wide range of operating conditions.
- Temperature and O_2 mole fraction fields are relatively uniform.
- NO_x emissions are always very low regardless of the combustor operating conditions

ARTICLE INFO

Article history:
Received 18 February 2012
Accepted 21 July 2012
Available online 31 July 2012

Keywords:
Experimental
Flameless oxidation
Pollutant emissions
Combustion efficiency

ABSTRACT

The aim of this study was to investigate experimentally the flameless oxidation phenomena. Experiments have been performed in a small-scale combustor fired with methane, and include detailed measurements of local mean temperatures and concentrations of major gas species for four representative combustor operating conditions, and flue-gas measurements for 27 operating conditions to quantify the combustor performance as a function of the excess air coefficient, inlet air velocity, fuel thermal input and preheat temperature of the combustion air. It was demonstrated that for the present combustor it is possible to establish flameless conditions over a wide range of operating conditions. The detailed in-combustor data show that the temperature and the O_2 mole fraction fields are relatively uniform, and that the maximum mean temperatures reached throughout the combustion chamber are relatively moderate, below 1500 °C, even under conditions in which the level of preheating of the combustion air is relatively high. The flue-gas data reveal that NO_x emissions are always very low regardless of the combustor operating conditions. However, the CO and HC emissions, and thus the combustion efficiency, are strongly affected by the levels of excess air and preheating of the combustion air. It was found that the combustion efficiency correlates reasonably well with the parameter $(T_{air}/T_{fuel}) \times (\dot{m}_{fuel}/\dot{m}_{air})$, varying linearly with it if its value is below ≈0.1 and remaining equal to approximately 100% otherwise.

1. Introduction

Flameless oxidation is a combustion regime where the reactants are highly diluted with hot combustion products, causing the reactions to occur in a distributed reaction zone with a reduced temperature maximum, smooth temperature gradients and low oxygen partial pressure. In this regime, distinct flame fronts, as they occur in typical lean premixed or diffusion flames, are replaced by a volume type flame mode. As a consequence, the temperature distribution is nearly uniform and NO_x emissions are very low. The reduction of the aero-acoustic fluctuations and extended stability limits are additional benefits of this combustion regime. This technology has received various names, such as high temperature air combustion (HiTAC) [1], flameless oxidation (FLOX®) [2], moderate or intense low oxygen dilution (MILD) combustion [3] and colorless distributed combustion (CDC) [4], with a number of studies revealing the success of this technology as a NO_x control technique.

Previous related experimental studies on this subject include those described in references 5 to 16, among others. Plessing et al. [5] reported instantaneous measurements of temperature and OH concentration from a combustion chamber and concluded that, under flameless oxidation conditions, combustion takes place in a regime similar to that of a well-stirred reactor, where no ignition and quenching events occur, which explains the low level of the combustion noise associated with this combustion regime. The measurements showed that the temperature rises smoothly and continuously along the furnace and that the OH is homogeneously distributed in the burnt side of the flame. The experimental results also showed that the flameless oxidation regime yields lower NO_x emissions as compared with conventional flames. Weber et al. [6] reported detailed measurements of velocity, temperature, gas

* Corresponding author. Tel.: +351 218417372.
E-mail address: mcosta@ist.utl.pt (M. Costa).

1359-4311/$ – see front matter © 2012 Elsevier Ltd. All rights reserved.
http://dx.doi.org/10.1016/j.applthermaleng.2012.07.027

species composition and radiation from flameless combustion in a natural gas-fired semi-industrial furnace, and concluded that the furnace was operating under conditions resembling a well-stirred reactor, with almost all furnace volume filled with combustion products containing 2–3% of O_2. Later on, Weber et al. [7] obtained results from the same facility that reveal the potential of this technology also for the combustion of liquid and solid fuels. Flamme [8] reported detailed measurements of temperature from a semi-industrial furnace operating under flameless oxidation conditions, with the results revealing the uniformity of the temperature field and showing the capacity to achieve low NO_x emissions using this technology even with high preheated air levels. Dally et al. [9] studied the effects of the fuel dilution with CO_2 and N_2, in a recuperative furnace, on the structure of the flameless oxidation. The results showed that the dilution of the fuel stream with inert gases may help to achieve flameless oxidation conditions and to reduce NO_x emissions. Simultaneous imaging of OH and temperature confirmed that the reaction zone is rather distributed under flameless oxidation conditions. Szegö et al. [10] reported measurements of temperature and flue-gas composition from a MILD laboratory combustion furnace. They found that air preheating is not required to achieve MILD combustion, even with 40% of useful heat being extracted through a cooling loop. Subsequently, Szegö et al. [11] investigated in the same furnace the operational characteristics of a parallel jet MILD combustion burner system. They found that a certain fuel jet momentum threshold was needed to achieve MILD conditions. This momentum ensured the penetration of the fuel jets to a region classified as the oxidation zone. More recently, Mi et al. [12] reported an investigation on the effects of the air–fuel injection momentum rate and the air–fuel premixing on the MILD combustion in a laboratory recuperative furnace. Various patterns of partially and fully premixed reactants have proven experimentally to work extremely well in the configuration studied. It was concluded that, above a critical momentum rate of the inlet fuel–air mixture below which MILD combustion cannot occur, both the inlet fuel–air mixedness and momentum rate impose insignificant influence on the stability of and emissions from the MILD combustion. Very recently, Veríssimo et al. [13] and Castela et al. [14] also examined the conditions required to establish MILD combustion in two small laboratory combustors, evidencing the importance of the excess air coefficient and of the inlet air velocity. Finally, in the context of multiple flameless combustion burners, the recent work of Danon et al. [15,16] must be mentioned. These authors presented an interesting study undertaken on a 300 kW furnace equipped with three pairs of regenerative flameless combustion burners, whose main objective was to optimize the furnace performance as a function of the burner configuration, firing mode, excess air and cycle time.

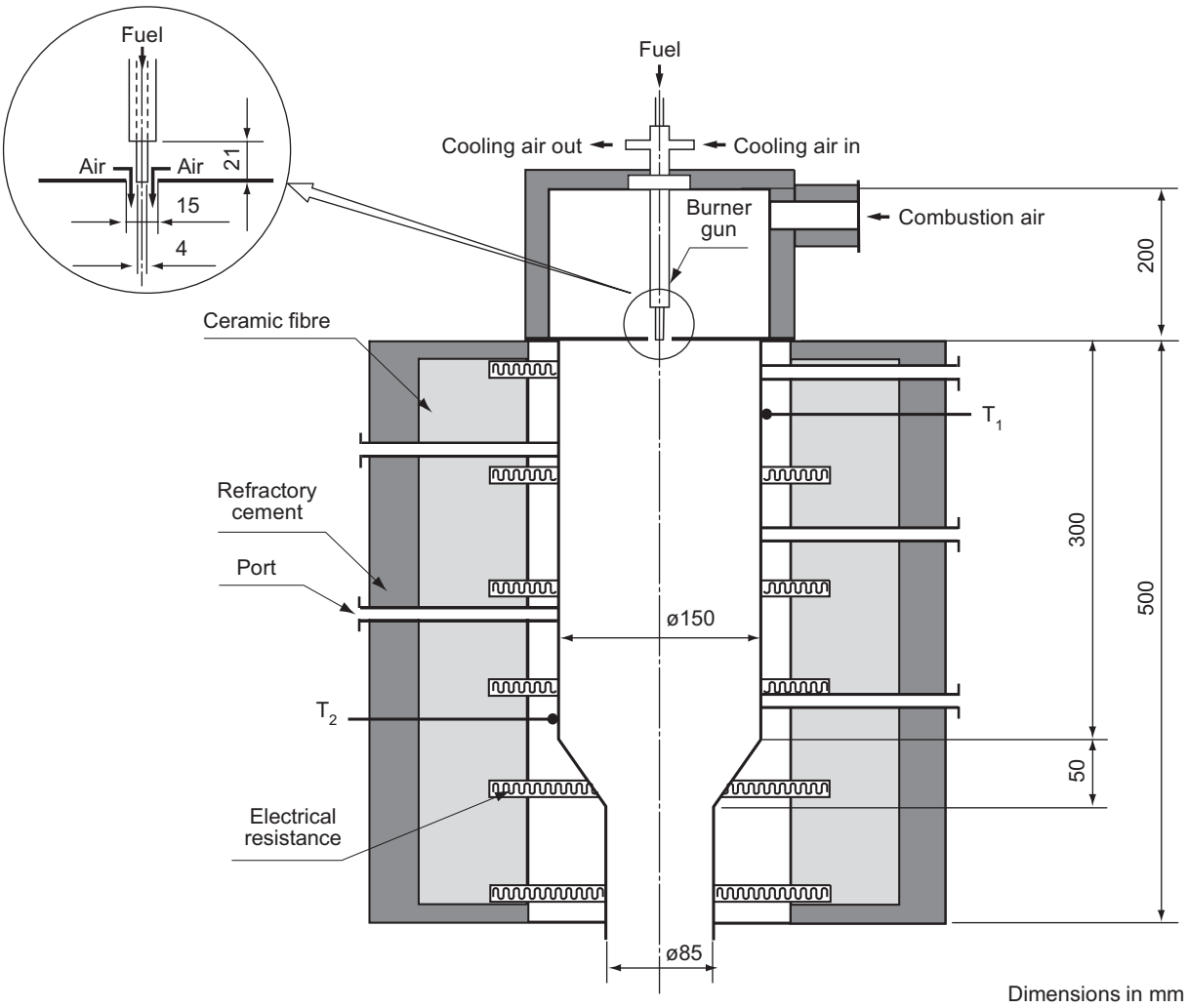

Fig. 1. Schematic representation of the small-scale combustor.

Despite the reasonable number of studies in the literature, the amount of detailed experimental data available for combustors operating under flameless conditions is relatively scarce and, in general, when reported, is for very few and narrow combustor operating conditions. The present investigation aims to extent the present data base on flameless oxidation and thereby to improve the understanding of the processes which occur during this combustion regime. To this end, experiments have been performed in a methane-fired small-scale combustor, and include detailed measurements of local mean temperatures and concentrations of major gas species for four representative combustor operating conditions, and flue-gas measurements for 27 operating conditions that allow to quantify the dependence of the NO_x emissions and combustion efficiency on the stoichiometry, inlet air velocity, fuel thermal input and preheat temperature of the combustion air.

2. Materials and methods

Fig. 1 shows schematically the combustor used in this study. The combustion chamber is a cylinder with an inner diameter of 150 mm and a length of 300 mm. The burner is placed at the top end of the combustion chamber and the exhaustion of the burned gases is at the bottom end through a convergent nozzle with a length of 50 mm and an angle of 35°. There are five ports along the length of the combustion chamber, each one with a diameter of 20 mm, which allow for the introduction of probes inside the combustion chamber. The combustion chamber is equipped with an electrical heating system that allows preheating the combustor walls up to ≈900 °C. Two thermocouples type K, installed in the combustion chamber as shown in Fig. 1 (T_1 and T_2), are used to monitor the wall temperatures and to evaluate the temperature gradients along the combustor. As seen in Fig. 1, the burner consists of a central gas gun (i.d. 4 mm, o.d. 6 mm) and a combustion air supply in a conventional double concentric configuration. A singular aspect of the present study is linked with the burner configuration, which has contiguous fuel and air inlets, in contrast with most previous studies where the fuel and air inlets are located well apart. In our combustor, the entrainment of combustion products in the air jet before combustion takes place, which is crucial to attain flameless conditions, is achieved by the high momentum of the air jet rather than by the distance between the air and fuel jets. The combustion air is preheated by an electrical heating system that allows inlet air temperatures up to 700 °C, which are monitored by a type K thermocouple installed in the wind box (not shown in Fig. 1).

Local mean temperature measurements were obtained using 76 μm diameter fine wire platinum/platinum: 13% rhodium thermocouples. The hot junction was installed and supported on 350 μm wires of the same material located in a twin-bore alumina sheath with an external diameter of 5 mm. The uncertainty due to radiation heat transfer was estimated to be less than 5% by considering the heat transfer by convection and radiation between the thermocouple bead and the surroundings.

The sampling of the gases for the measurement of local mean O_2, CO, CO_2, unburned hydrocarbons (HC) and NO_x concentrations was achieved using a stainless steel water-cooled probe. It was composed of a central 2 mm internal diameter tube through which quenched samples were evacuated. This central tube was surrounded by two concentric tubes for probe cooling. The gas sample was drawn through the probe and part of the system by an oil-free diaphragm pump. A condenser removed the main particulate burden and condensate. A filter and a drier removed any residual particles and moisture so that a constant supply of clean dry combustion gases was delivered to the analyzers through a manifold to give species concentration on a dry basis. The analytical instrumentation included a magnetic pressure analyzer for O_2 measurements, a non-dispersive infrared gas analyzer for CO_2 and CO measurements, a flame ionization detector for HC

Table 1
Test conditions.[a]

Run	Thermal input (kW)	Excess air coefficient	Inlet air velocity (m/s)	Inlet air temperature (°C)	Inlet fuel velocity (m/s)	Temperature T_1 (°C) – see Fig. 1	Temperature T_2 (°C) – see Fig. 1	Flue-gas temperature (°C)
1	13	1.2	89	590	31.8	900	–	–
2	13	1.3	92	551	31.8	900	–	–
3	13	1.4	95	540	31.8	900	–	–
4	13	1.5	109	570	31.8	900	–	–
5	13	1.6	111	543	31.8	900	–	–
6	13	2.0	139	538	31.8	900	–	–
7	10	1.1	73	720	24.4	949	950	1396
8[b]	10	1.6	103	700	24.4	901	911	1271
9[b]	10	2.0	128	700	24.4	900	900	1212
10	10	2.3	147	700	24.4	900	900	1197
11	10	2.5	160	700	24.4	900	900	1146
12[b, c]	15.6	1.6	155	700	38.1	988	980	1355
13	12	1.6	120	700	29.3	950	957	1338
14	10	1.6	103	700	24.4	901	911	1271
15	8	1.6	82	700	19.6	900	900	1278
16	15.6	1.6	155	700	38.1	988	980	1355
17	12	2.0	153	700	29.3	930	930	1263
18	10	2.5	160	700	24.4	900	900	1146
19	8	3.2	164	700	19.6	900	900	935
20	10	1.6	103	700	24.4	901	911	1271
21	10	1.6	90	600	24.4	900	910	1265
22	10	1.6	82	500	24.4	900	908	1256
23	10	1.6	70	400	24.4	900	905	1220
24	10	1.6	103	700	24.4	901	911	1271
25	10	1.7	100	600	24.4	900	905	1250
26[b, c]	10	2.0	102	500	24.4	899	901	1187
27	10	2.3	104	400	24.4	900	898	990

[a] For all conditions: inlet fuel temperature = 20 °C.
[b] Measurements of axial temperature and major gas species mole fraction profiles.
[c] Measurements of radial temperature and major gas species mole fraction profiles.

measurements and a chemiluminescent analyzer for NO_x measurements. Zero and span gas calibration with standard mixtures were performed before and after each measurement session. The major sources of uncertainty in the concentration measurements inside the combustor were associated with the quenching of chemical reactions and aerodynamic disturbances of the flow. Quenching of the chemical reactions was rapidly achieved upon the samples being drawn into the central tube of the probe due to the high water cooling rate in its surrounding annulus. No attempt was made to quantify the probe flow disturbances. On average, the repeatability of the gas species concentration data was within 10% of the mean value.

Flue-gas data were obtained using also the procedures described above for the in-combustor data collection. At the combustor exit, probe effects were negligible and errors arose mainly from quenching of chemical reactions, which was found to be adequate. Repeatability of the flue-gas data was, on average, within 5% of the mean value.

3. Results and discussion

The experiments performed in the small-scale combustor (Fig. 1), fired with methane, included initially detailed flue-gas measurements for 27 combustor operating conditions, as summarized in Table 1. Runs 1 to 11 allow quantifying the effect of the excess air coefficient on the combustor performance; runs 12 to 15 and runs 16 to 19 allow quantifying the effect of the fuel thermal input while maintaining constant the excess air coefficient and (approximately) the inlet air velocity, respectively; and, finally, runs 20 to 23 and runs 24 to 27 allow quantifying the effect of the inlet air temperature while maintaining constant the excess air coefficient and (approximately) the inlet air velocity, respectively. Subsequently, detailed in-combustor measurements of local mean temperature and gas species concentrations of O_2, CO_2, CO, HC and NO_x for four representative combustor operating conditions (runs 8, 9, 12 and 26 in Table 1) have also been performed.

3.1. General aerodynamic characteristics of the present flames

In order to help the understanding of the discussion of the results presented below, Fig. 2 shows the gas flow pattern for run 26 listed in Table 1, as predicted in a parallel modeling study [17]. The high momentum of the air jet originates a long recirculation zone that extends up to the exit section of the combustor. Note that the computational domain extends into the exhaust duct, which is not shown in Fig. 2, so that the predictions are not influenced by the exit boundary condition. Hot combustion products entrain into the recirculation zone, transporting momentum and energy to this region. The hot temperature of the combustor walls contributes to maintain the temperature and species concentration fields relatively uniform. The computed recirculation rate, as defined in Wünning and Wünning [2], is 1.9. The high recirculation ratio promotes significant mixing between the air and the recirculated combustion products prior to reaction with the fuel, which is a key feature of the flameless oxidation regime.

In the present study, visual observation through the inspection ports revealed that there was no visible flame for the combustor operating conditions examined. It was also observed that combustion was stable, with very low noise. The results presented in Section 3.2 show no evidence of temperature or CO peaks (flame front). Finally, the NO and CO emissions presented in Section 3.3 are quite low. All these observations and results indicate that the combustor was operating under flameless combustion conditions.

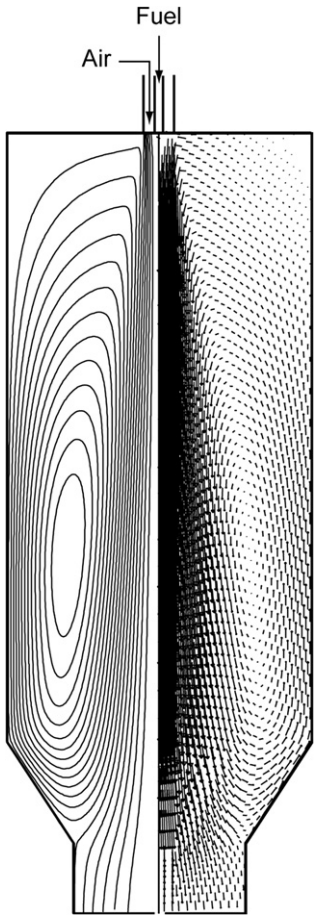

Fig. 2. Predicted flow pattern for run 26 listed in Table 1.

3.2. In-combustor measurements

Fig. 3 shows the axial temperature profiles for runs 8, 9, 12 and 26, Fig. 4 shows the axial O_2 and CO_2 mole fraction profiles also for runs 8, 9, 12 and 26 and Fig. 5 shows the axial CO and HC mole fraction profiles for the same four runs. Data for in-combustor NO_x

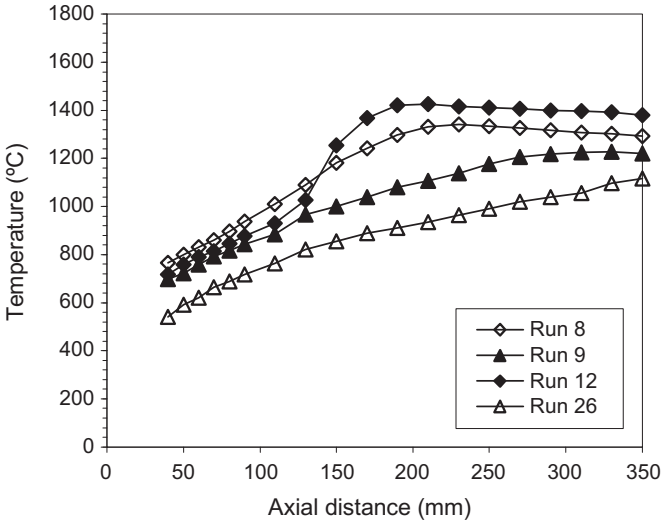

Fig. 3. Axial temperature profiles for runs 8, 9, 12 and 26.

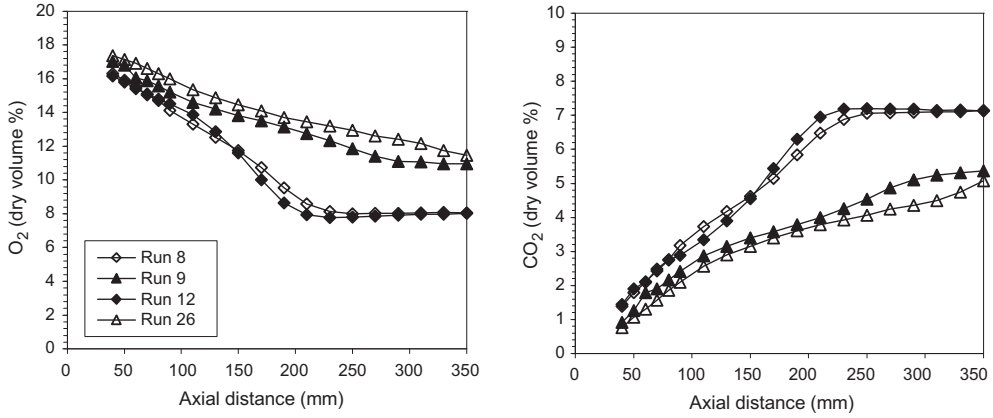

Fig. 4. Axial O_2 and CO_2 mole fraction profiles for runs 8, 9, 12 and 26.

mole fractions are not showed owing to the very low measured values throughout the combustor in agreement with the very low NO_x emissions reported below. Altogether runs 8, 9, 12 and 26 allow examining the effects of the excess air coefficient, fuel thermal input and inlet air temperature on the combustor performance.

Fig. 3 reveals that the increase in the excess air level from run 8 to 9 yielded lower gradients in the axial temperature profile and reduced temperature values. In run 9 ($\lambda = 2$) the temperature maximum is located in a position closer to the combustor exit and presents a lower value than in run 8 ($\lambda = 1.6$). These results indicate that in run 9 the combustion process is less intense and distributed over a larger volume of the combustion chamber than in run 8.

A comparison between the axial temperature profiles of runs 8 and 12 (Fig. 3) indicates that the fuel thermal input changes qualitatively the shape of the profile in the near burner zone. In run 8 (thermal input = 10 kW) the temperature increases linearly in the first 200 mm from the burner, while in run 12 (thermal input = 15.6 kW) the temperature profile presents an inflection point at $x \approx 140$ mm (x is the distance from the burner) and a steeper gradient in the region situated between $x = 140$ and 180 mm. The inflection point indicates that it is here that the combustion process becomes more intense. In both runs the temperature maxima are located at about the same position being the temperature evolution after the maxima very similar for both runs, with a smooth decrease in the temperature towards the combustor exit. The temperature maximum and the temperatures measured in the lower part of the combustor are, however, higher in run 12.

The on-axis temperature data measured for runs 9 and 26 indicate that the inlet air temperature and the inlet air velocity do not affect significantly the temperature evolution along the combustor. In fact, the difference between the measured temperatures in runs 9 and 26 is nearly constant and roughly equal to the difference of the inlet air temperatures of the two runs.

Fig. 4 reveals that the CO_2 mole fraction profiles present qualitatively the same trends as those of the temperature, being the O_2 mole fraction profiles complementary of those of the CO_2. The results reveal that the axial evolution of the O_2 and CO_2 mole fractions are mainly influenced by the excess air. In runs 9 and 26 (both with $\lambda = 2$) the CO_2 mole fractions increase continuously and approximately linearly until the end of the combustion chamber and the O_2 mole fractions decrease in a similar way. In runs 8 and 12 the CO_2 mole fractions increase up to $x = 200$ mm, beyond which they remain constant until the exit of the combustor. The O_2 mole fractions present a complementary evolution. These results, together with the temperature profiles shown in Fig. 3, indicate that in runs 8 and 12 the combustion process occurs mainly during the first 200 mm of combustion chamber, while in runs 9 and 26 the combustion process develops over a larger volume of the combustion chamber.

The fuel thermal input affects only marginally the evolution of the on-axis O_2 and CO_2 mole fractions (comparison between runs 8 and 12). However, the profiles of O_2 and CO_2 mole fractions present an inflection point for both runs 8 and 12, as observed earlier in the corresponding temperature profile of run 12, but in contrast with run 8 (see Fig. 3).

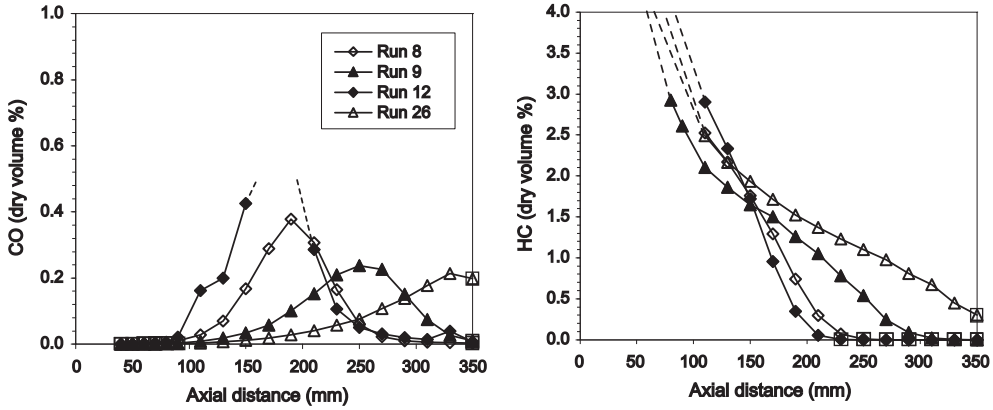

Fig. 5. Axial CO and HC mole fraction profiles for runs 8, 9, 12 and 26.

The level of preheating of the combustion air has also a small influence in the evolution of the O_2 and CO_2 mole fraction profiles (comparison between runs 9 and 26). In fact, the profiles for runs 9 and 26 are rather similar. In run 9, where the inlet air temperature is higher, the O_2 and CO_2 mole fractions reach values analogous to those measured at the exhaust of the combustor, while in run 26 the O_2 and CO_2 mole fractions reveal a tendency to decrease and increase, respectively, up to the exit of the combustor.

Fig. 5 shows that in runs 8 and 12 the HC mole fractions decrease approximately linearly until zero at $x \approx 200$–225 mm. These runs present a similar evolution of the CO mole fractions – note that in run 12 the region situated between $x = 150$ and 200 mm presents CO mole fraction values that exceeded the upper range of the analyzer used (0.5%). The fuel thermal input has a reduced influence in the HC mole fraction profiles. However, run 12, which has the higher fuel thermal input, presents a higher gradient in the region between $x = 120$ and 180 mm, as also observed earlier for the temperature and the O_2 and CO_2 mole fractions.

A comparison between runs 8 and 9 indicates that increasing the excess air, while maintaining constant the fuel thermal input and the inlet air temperature, smoothes the CO and HC mole fraction profiles and distributes the CO and HC mole fractions over a larger volume of the combustion chamber. In run 9 the CO appears in the combustion chamber further downstream than in run 8, reaching values close to zero only near the combustor exit. The HC oxidation also ends later in the combustion chamber for run 9. These results clearly indicate that the combustion process in run 9 is distributed over a larger volume of the combustion chamber than in run 8.

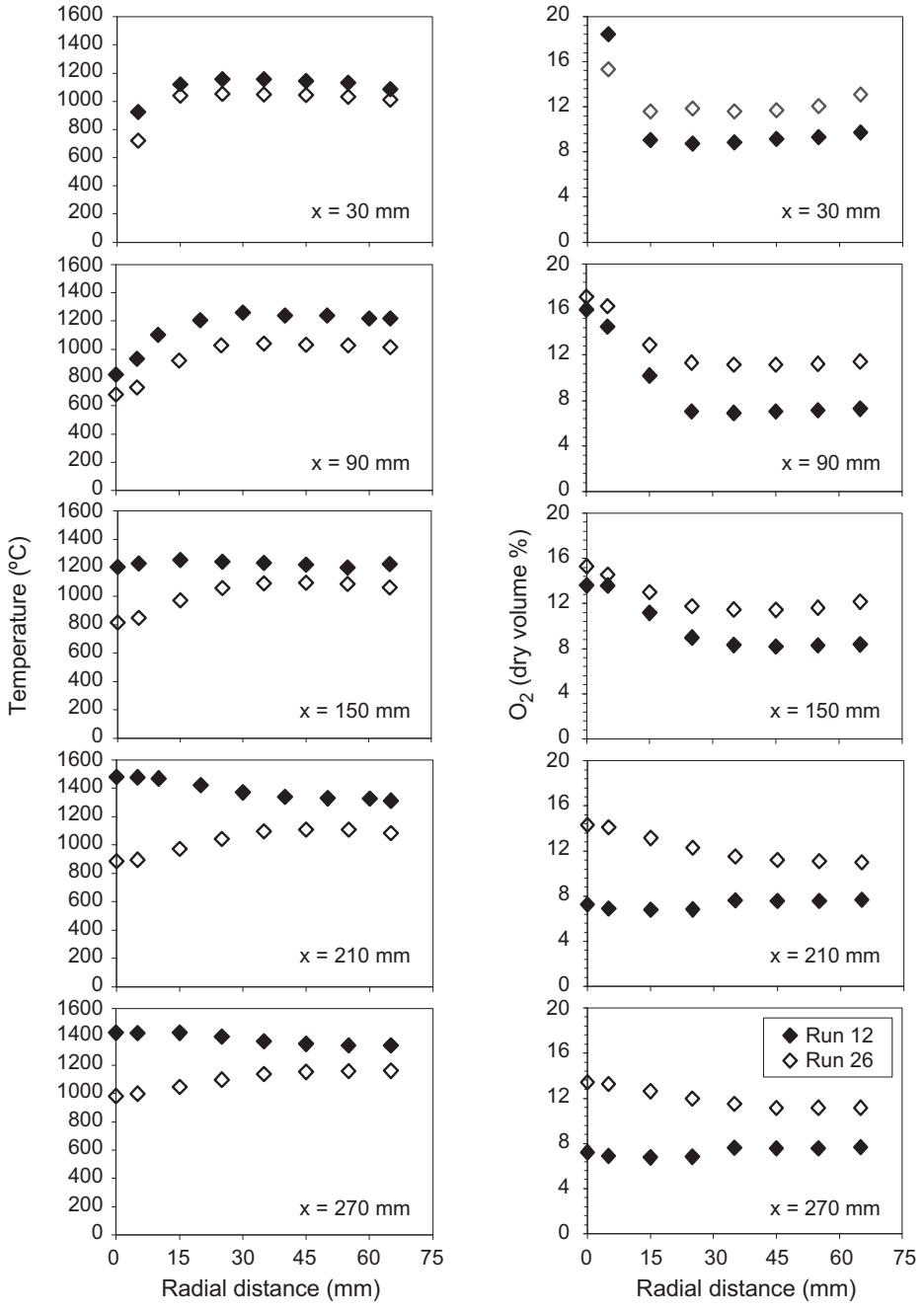

Fig. 6. Radial temperature (left) and O_2 mole fraction (right) profiles for runs 12 and 26.

Finally, a comparison between runs 9 and 26 indicates that reducing the inlet air temperature creates an effect similar to that of increasing the excess air, that is, the CO and HC mole fraction profiles present smoother evolutions and the CO appears in the combustion chamber further downstream. The results for run 26 clearly show that the reaction zone extends beyond the end of the combustor, as evidenced by the HC and CO emissions measured for this run.

The measurements of temperature and gas species mole fractions give a clear indication of the extension of the reaction zone. The results demonstrate that, under flameless conditions, the combustion process is distributed over a large volume of the combustor. The axial evolution of the temperatures and major gas chemical species is rather smooth. The maximum temperatures measured are relatively moderate, even when the level of preheating of the combustion air is relatively high.

The results obtained suggest that, amongst the parameters studied, the excess air coefficient is the one that affects most the reaction zone. It was concluded that an increase in excess air reduces the combustion intensity and extends the reaction zone over a larger volume of the combustion chamber.

The fuel thermal input changes slightly the axial temperature profile but, overall, has a reduced influence on the combustion process as concluded from the axial gas species mole fraction profiles.

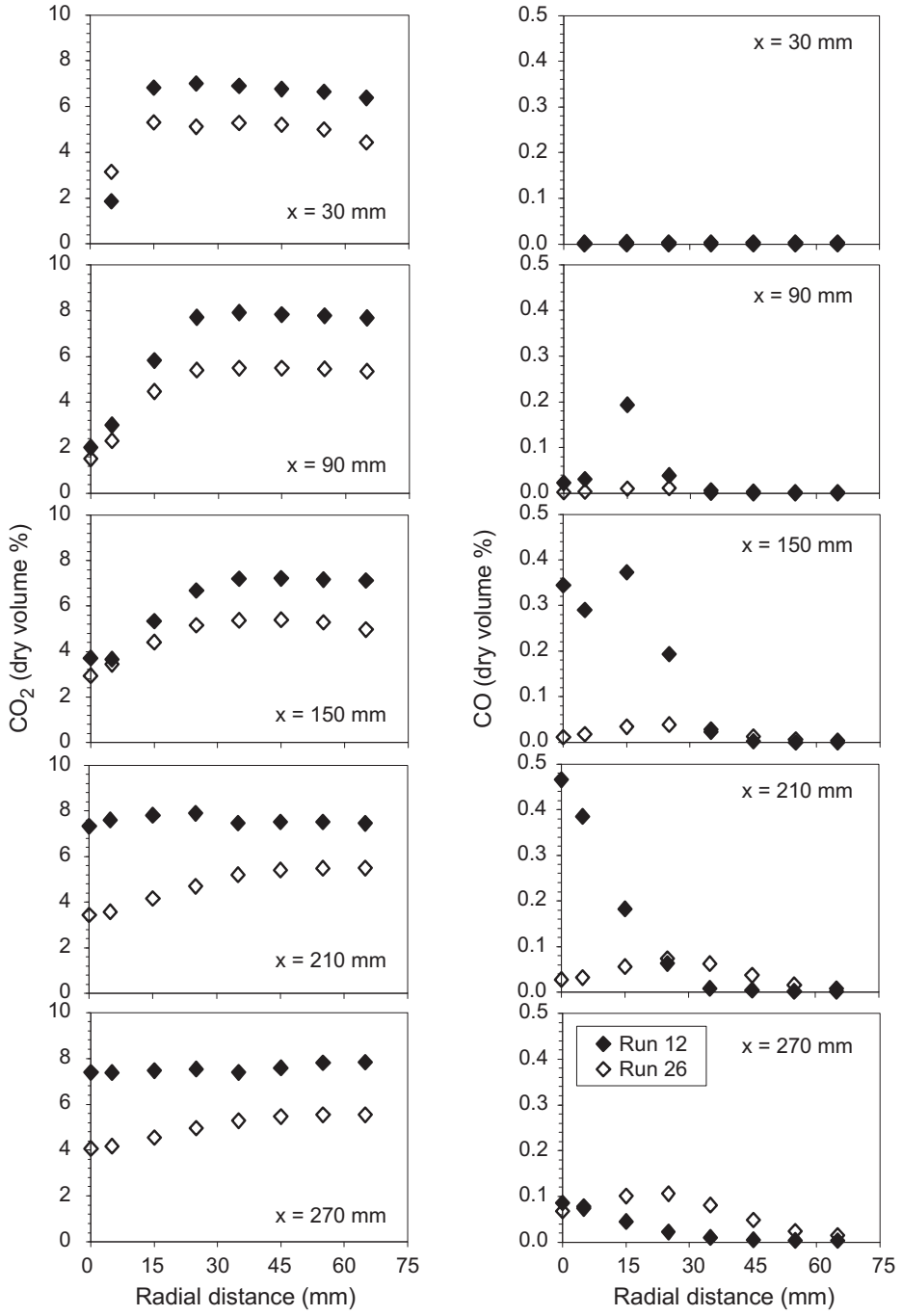

Fig. 7. Radial CO_2 mole fraction (left) and CO mole fraction (right) profiles for runs 12 and 26.

The reduction of the level of preheating of the combustion air lowers the temperature along the axis of the combustion chamber and smoothes the axial HC and CO mole fractions profiles. The decrease in the temperature reduces the reaction rates and slows down the combustion process.

In order to enhance the knowledge that emerged from the measurements of the temperature and gas species mole fractions along the combustor axis for runs 8, 9, 12 and 26, these trials were complemented by detailed combustion measurements throughout the combustor for runs 12 and 26 (see Table 1). Fig. 6 shows the radial temperature and O_2 mole fraction profiles, Fig. 7 shows the radial CO_2 and CO mole fraction profiles and Fig. 8 shows the radial HC and NO_x mole fraction profiles for these two runs.

Fig. 6 shows that the radial temperature profiles are extremely homogeneous, with the exception of the measured profiles in the near burner region. At $x = 30$ and 90 mm the temperature profiles illustrate clearly the expansion of the central jet. This is the region where intense mixing between the fuel, the combustion air and the recirculated flue-gases takes place. Here the temperature profiles are rather homogeneous, being the O_2 mole fraction profiles less homogeneous due to the high momentum of the central jet.

In the recirculation zone (see also Fig. 2), the temperature and O_2 mole fraction profiles are fairly uniform and, in the case of the oxygen, the values are similar to those measured in the flue-gases. In the case of the temperature, the profiles measured in the recirculation zone near the top of the combustion chamber reveal lower

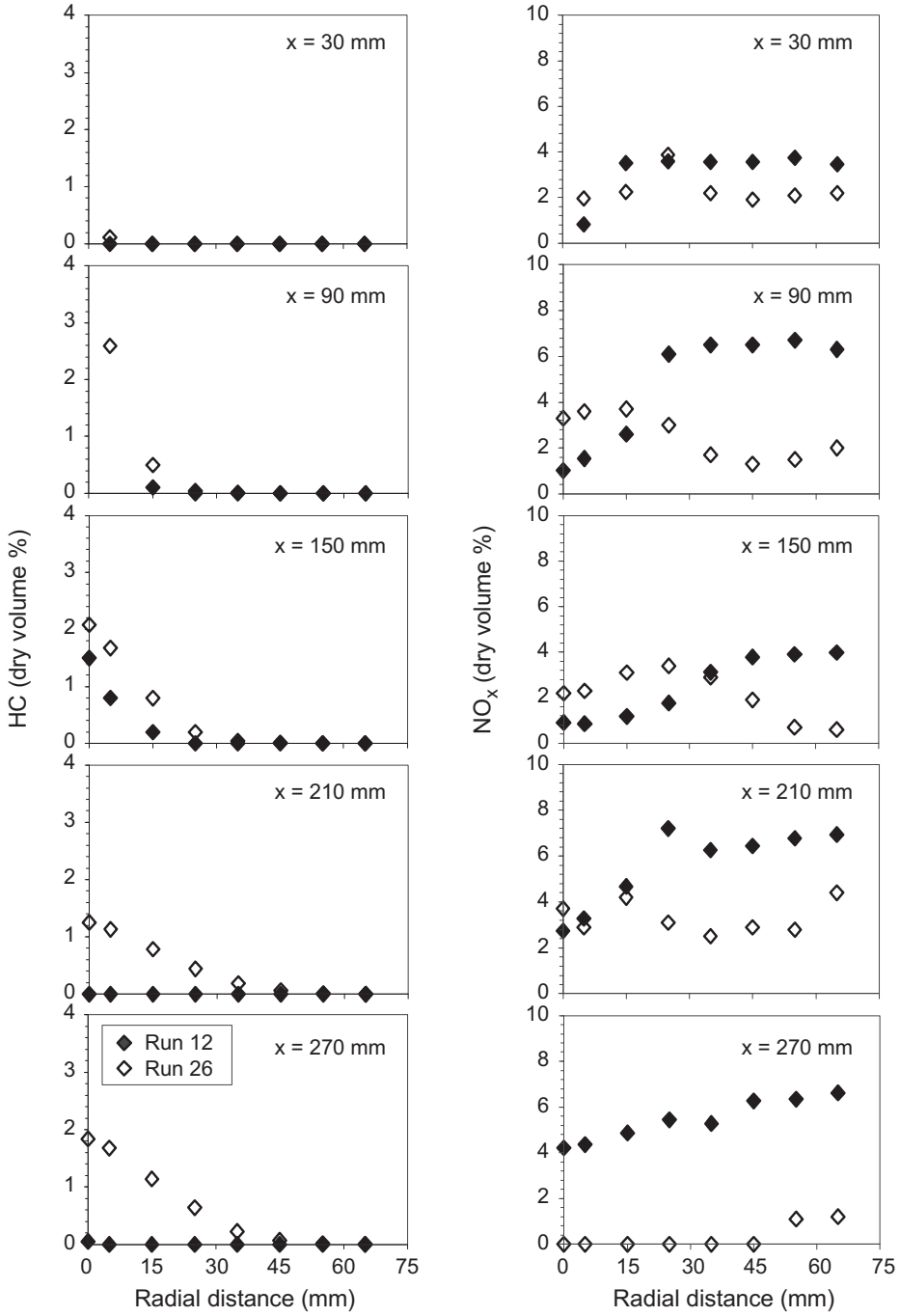

Fig. 8. Radial HC mole fraction (left) and NO_x mole fraction (right) profiles for runs 12 and 26.

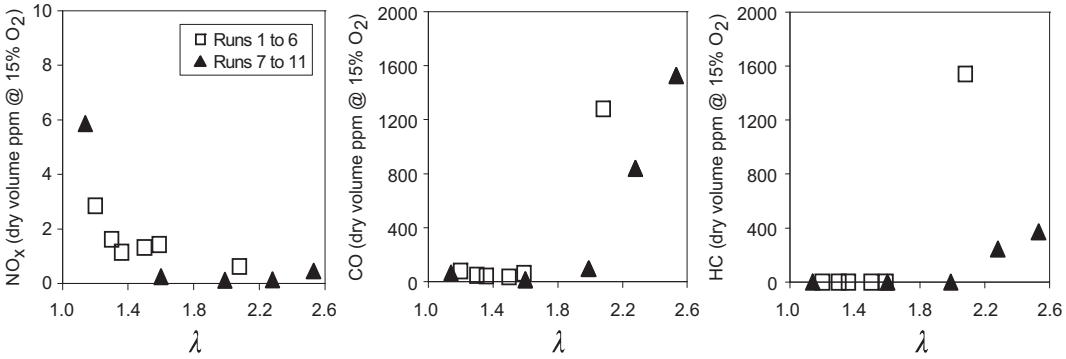

Fig. 9. Effect of the excess air coefficient (λ) on NO_x, CO and HC emissions.

values than those registered in the flue-gases. This is due to the heat losses along the walls of the combustor from the hot recirculated gases. This situation is clearer in run 12, where the measured temperatures are higher, which explains why at $x = 30$ mm the measured temperatures are similar for both runs while at $x = 270$ mm the measured temperatures in run 12 are much higher than those measured in run 26.

Fig. 7 indicates that the evolutions of O_2 and CO_2 mole fractions are complementary. With the exception of the profiles measured at $x = 150$ mm in run 12, where the temperature profile is nearly homogeneous and the CO_2 mole fractions still show a slight gradient near the combustor axis, the CO_2 mole fractions exhibit an evolution qualitatively comparable to that of the temperatures. A comparison between the profiles measured in the near burner region discloses that the evolution is similar for both runs. In this region, the gradient of the CO_2 mole fraction profiles near the combustor axis is smooth. In the recirculation zone, the profiles are uniform and differ only because of the different excess air. At the end of the combustion chamber the CO_2 mole fraction profiles for run 12 are uniform while those for run 26 still present a small gradient.

Fig. 7 reveals that the CO mole fractions are always <0.5%. The CO mole fraction profiles for run 26 are more homogeneous than those for run 12. In run 12, at $x = 90$ mm, CO appears in the zone of interaction between the central jet and the recirculation zone. At $x = 150$ and 210 mm, with the progress of the combustion process, there is an increase in the CO mole fractions near the combustor axis, which is subsequently converted to CO_2 as confirmed at $x = 270$ mm.

The radial CO mole fraction profiles support the conclusions drawn from the axial CO profiles. In run 26 the CO appears in regions closer to the combustor exit than in run 12, being the values lower. The lower CO mole fraction values measured in run 26 are partly due to the effect of the dilution promoted by the higher excess air. On the other hand, the axial CO mole fraction profile indicates that in run 26 the CO formation occurs mainly at the end of the combustor beyond $x = 270$ mm.

Fig. 8 reveals that the HC and CO mole fraction profiles for runs 12 and 26 present a qualitatively similar behavior. Note that at $x = 90$ mm it was not possible to measure the HC mole fraction around the combustor axis because it exceeded the maximum range of the HC analyzer (0.5%). As suggested by the axial HC mole fraction profiles, the radial HC profiles confirm that the combustion process in run 26 is distributed over a larger volume of the combustion chamber than in run 12, reaching regions beyond the combustor exit, already in the exhaust duct. The NO_x mole fractions measured throughout the combustor are extremely low and are consistent with the measured values in the flue-gases. In fact, the temperature measurements indicate that they only exceed 1400 °C in run 12, which explains the very low measured NO_x levels.

3.3. Flue-gas measurements

Fig. 9 shows the effect of the excess air coefficient (λ) on NO_x, CO and HC emissions for two series of runs (runs 1 to 6 and runs 7 to 11 – see Table 1). In runs 1 to 6 the fuel thermal input was 13 kW and the inlet air temperature varied between 538 °C and 590 °C, while in runs 7 to 11 the fuel thermal input was 10 kW and the inlet air temperature varied between 700 °C and 720 °C. It is observed that NO_x emissions are extremely low (<6 ppm@15% O_2) for both thermal inputs, as expected for flameless oxidation conditions, even near stoichiometry with a relatively high level of air preheating. Both CO and HC emissions have the same trends, i.e., they are extremely low for small values of λ. However, for values of $\lambda > 2$, CO and HC emissions become important and have a linear increase with the value of λ. This is because an increase in the excess air level

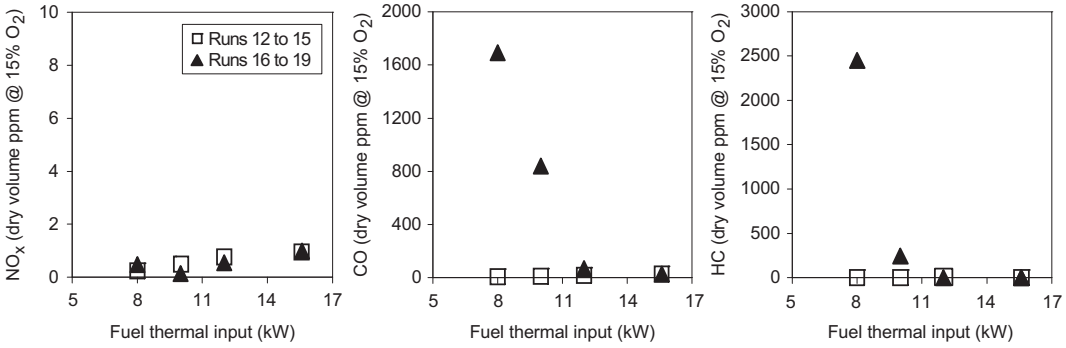

Fig. 10. Effect of the fuel thermal input on NO_x, CO and HC emissions.

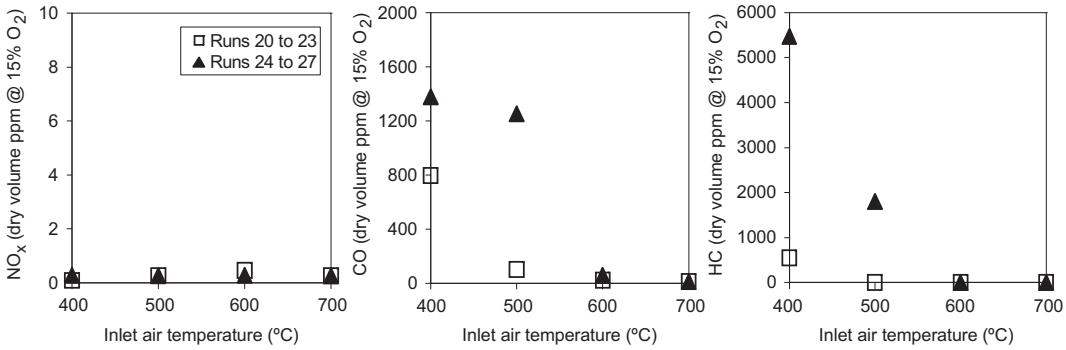

Fig. 11. Effect of the inlet air temperature on NO_x, CO and HC emissions.

causes a reduction in the temperature inside the combustor, as typified by the temperature of the exhaust gases displayed in Table 1, which slows down the reaction rate and hence increases the level of CO and HC emissions.

Fig. 10 shows the effect of the fuel thermal input on NO_x, CO and HC emissions for two series of runs (runs 12 to 15 and runs 16 to 19 – see Table 1). In runs 12 to 15 the variations in fuel thermal input are accompanied by variations in the inlet air velocity while maintaining constant the level of excess air, whereas in runs 16 to 19 the variations in fuel thermal input are accompanied by variations in the excess air level while maintaining approximately constant the inlet air velocity. In all these runs the inlet air temperature was kept equal to 700 °C. It is seen that NO_x emissions are extremely low regardless of the fuel thermal input. This suggests that, under flameless oxidation conditions, the thermal density in the combustor does not affect the NO_x emissions. The emissions of CO and HC are important for the smaller values of the fuel thermal input. The reduction of the thermal density in the combustor for higher excess air levels and smaller thermal inputs, as typified by the temperature of the exhaust gases displayed in Table 1, causes a reduction of the temperature inside the combustor. This slows down the reaction rates and increases the emissions of CO and HC.

Fig. 11 shows the effect of the combustion inlet air temperature on NO_x, CO and HC emissions for two series of runs (runs 20 to 23 and runs 24 to 27 – see Table 1). In runs 20 to 23 the variations in the inlet air temperature are accompanied by variations in the inlet air velocity while maintaining constant the level of excess air, whereas in runs 24 to 27 the variations in the inlet air temperature

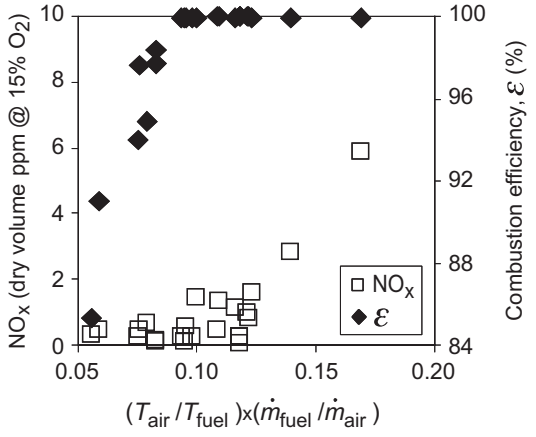

Fig. 12. NO_x emissions and combustion efficiency as a function of the parameter $(T_{air}/T_{fuel}) \times (\dot{m}_{fuel}/\dot{m}_{air})$.

are accompanied by variations in the excess air level while maintaining constant the inlet air velocity. In all these runs the fuel thermal input was kept equal to 10 kW. The results show that, under flameless oxidation conditions, the inlet air temperature has no effect on the very low NO_x emissions. The results also show that above 600 °C the inlet air temperature has no significant effects on CO and HC emissions. For lower values of the inlet air temperature, CO emissions become significant and HC emissions extremely high. The reduction of the inlet air temperature reduces the temperature inside the combustion chamber, which slows down the oxidation of the fuel, causing CO and HC emissions to increase.

Fig. 12 shows the effect of the parameter $(T_{air}/T_{fuel}) \times (\dot{m}_{fuel}/\dot{m}_{air})$ on NO_x emissions and combustion efficiency. Note that the data presented in Fig. 12 includes all the experimental conditions analyzed in this study. Combustion efficiency is defined here as $\varepsilon = 100 \times [1 - EI_{CO} \times (\Delta H_{CO}/\Delta H_{CH4}) - EI_{HC}]$, where the emissions are expressed in terms of the emission index (EI) and ΔH_i is the lower heating value of species i. The results show that the parameter $(T_{air}/T_{fuel}) \times (\dot{m}_{fuel}/\dot{m}_{air})$ correlates well with the combustion efficiency and reasonably well with the NO_x emissions. For values of $(T_{air}/T_{fuel}) \times (\dot{m}_{fuel}/\dot{m}_{air})$ greater than ≈ 0.1 the combustion efficiency is 100% and the NO_x emissions increase linearly while for lower values of that parameter the combustion efficiency changes linearly and the NO_x emissions are constant and close to zero. Small values of $\dot{m}_{fuel}/\dot{m}_{air}$ represent large values of λ, which together with the small values of the inlet air temperature, reduce the temperature inside the combustion chamber. Therefore the reaction rate decreases, both the CO and HC emissions increase and both the combustion efficiency and the NO_x emissions decrease. For higher values of $(T_{air}/T_{fuel}) \times (\dot{m}_{fuel}/\dot{m}_{air})$ the NO_x emissions increase slightly presumably because of the higher in-combustor temperatures.

4. Conclusions

Measurements have been obtained in a methane-fired small-scale combustor operating under flameless conditions. The results include detailed measurements of local mean temperatures and concentrations of major gas species for four representative combustor operating conditions, and flue-gas measurements for 27 operating conditions to quantify the combustor performance as a function of the excess air coefficient, inlet air velocity, fuel thermal input and preheat temperature of the combustion air. For the present combustor configuration it was demonstrated that it is possible to establish flameless conditions over a wide range of operating conditions. The detailed in-combustor data disclose that the temperature, carbon dioxide and oxygen molar fraction fields are relatively uniform, without the large gradients typically observed in conventional flames. The temperature, CO_2 and O_2

mole fraction profiles present, however, a lower uniformity in the vicinity of the air injection. The in-combustor data also reveal that the maximum mean temperatures reached throughout the combustion chamber are relatively moderate, below 1500 °C, even under conditions in which the level of preheating of the combustion air is relatively high. The flue-gas data reveal that NO_x emissions are always low regardless of the combustor operating conditions. However, the CO and HC emissions, and thus the combustion efficiency, are strongly affected by the levels of excess air and preheating of the combustion air. It was found that the combustion efficiency correlates reasonably well with the parameter $(T_{air}/T_{fuel}) \times (\dot{m}_{fuel}/\dot{m}_{air})$, varying linearly with it if its value is below ≈ 0.1 and remaining equal to approximately 100% otherwise.

Acknowledgements

This work was developed within the framework of project PPCDT/EME/57480/2004, which is financially supported by Fundação para a Ciência e a Tecnologia (FCT). A. Rebola is pleased to acknowledge the FCT for the provision of a scholarship (SFRH/BD/23619/2005).

References

[1] M. Katsuki, T. Hasegawa, The science and technology of combustion in highly preheated air, Proc. Combust. Inst. 27 (1998) 3135–3146.
[2] J.A. Wünning, J.G. Wünning, Flameless oxidation to reduce thermal NO-formation, Prog. Energy Combust. Sci. 23 (1997) 81–94.
[3] A. Cavaliere, M. de Joannon, Mild combustion, Prog. Energy Combust. 30 (2004) 329–366.
[4] V.H. Arghode, A.K. Gupta, Effect of flow field for colorless distributed combustion (CDC) for gas turbine combustion, Appl. Energy 87 (2010) 1631–1640.
[5] T. Plessing, N. Peters, J.G. Wünning, Laseroptical investigation of highly preheated combustion with strong exhaust gas recirculation, Proc. Combust. Inst. 27 (1998) 3197–3204.
[6] R. Weber, S. Orsino, N. Lallemant, A. Verlaan, Combustion of natural gas with high-temperature air and large quantities of flue gas, Proc. Combust. Inst. 28 (2000) 1315–1321.
[7] R. Weber, J.P. Smart, W. Kamp, On the (MILD) combustion of gaseous, liquid, and solid fuels in high temperature preheated air, Proc. Combust. Inst. 30 (2005) 2623–2629.
[8] M. Flamme, New combustion systems for gas turbines (NGT), Appl. Therm. Eng. 24 (2004) 1551–1559.
[9] B.B. Dally, E. Riesmeier, N. Peters, Effect of fuel mixture on moderate and intense low oxygen dilution combustion, Combust. Flame 137 (2004) 418–431.
[10] G.G. Szegö, B.B. Dally, G.J. Nathan, Scaling of NO_x emissions from a laboratory-scale mild combustion furnace, Combust. Flame 154 (2008) 281–295.
[11] G.G. Szegö, B.B. Dally, G.J. Nathan, Operational characteristics of a parallel jet MILD combustion burner system, Combust. Flame 156 (2009) 429–438.
[12] J. Mi, P. Li, B.B. Dally, R.A. Craig, Importance of initial momentum rate and air–fuel premixing on moderate or intense low oxygen dilution (MILD) combustion in a recuperative furnace, Energy Fuels 23 (2009) 5349–5356.
[13] A.S. Veríssimo, A.M.A. Rocha, M. Costa, Operational, combustion and emission characteristics of a small-scale combustor, Energy Fuels 25 (2011) 2469–2480.
[14] M. Castela, Veríssimo, A.M.A. Rocha, M. Costa, Experimental study of the combustion regimes occurring in a laboratory combustor, Combust. Sci. Technol. 184 (2012) 243–258.
[15] B. Danon, E.-S. Cho, W. de Jong, D.J.E.M. Roekaerts, Parametric optimization study of a multi-burner flameless combustion furnace, Appl. Therm. Eng. 31 (2011) 3000–3008.
[16] B. Danon, E.-S. Cho, W. de Jong, D.J.E.M. Roekaerts, Numerical investigation of burner positioning effects in a multi-burner flameless combustion furnace, Appl. Therm. Eng. 31 (2011) 3885–3896.
[17] A. Rebola, P.J. Coelho, M. Costa, On Methane Flameless Combustion. Proceedings of the 10th International Conference on Energy for a Clean Environment, Lisboa, Portugal, 7–10 July; 2009.